

Elastic Scattering of Heavy Ions and Nucleus–Nucleus Potential with a Repulsive Core

V. Yu. Denisov and O. I. Davidovskaya

*Institute for Nuclear Research, National Academy of Sciences of Ukraine, Kiev, UA-03680 Ukraine
e-mail: denisov@kinr.kiev.ua*

Abstract—Elastic scattering of $^{12}\text{C} + ^{12}\text{C}$ at 139.5, 158.8 MeV and $^{16}\text{O} + ^{12}\text{C}$ at 132, 169 MeV was analyzed in the framework of an optical model using the repulsive-core nucleus–nucleus potential. Calculations with and without consideration of the core were performed and the influence of the core on the elastic scattering cross section was analyzed. It was shown that taking account of the core leads to an increase in the elastic scattering cross section for backward angles. The decomposition of the scattering amplitude into nearside and far-side components was studied.

DOI: 10.3103/S1062873810040325

INTRODUCTION

The potential of nucleus–nucleus interaction is a key component in any analysis of nuclear reactions. The potential of interaction between nuclei can be used to estimate the cross-sections of different nuclear reactions [1]. The potential consists of nuclear, Coulomb, and centrifugal components. The Coulomb and centrifugal interactions of two nuclei are well known, but the nuclear component of nuclear–nuclear interaction is not so well known.

Macroscopic, semi-microscopic, and microscopic approaches have been used to estimate the nucleus–nucleus potential [1–15]. The nuclear component of the interaction potential is often parameterized by the Woods–Saxon potential [1]. The parameters of the phenomenological potential are found by the fitting of experimental data on different reactions. The parameters of this potential therefore depend on the reaction channel and the model applied for the description of the reaction. The potential “proximity” [2] is obtained within the framework of a macroscopic approximation using the properties of nuclear matter, nuclear surface, density distribution in nuclei, and nucleon–nucleon interaction.

Semi-microscopic and microscopic models for calculating nuclear–nuclear potential are based on Skyrme nucleon–nucleon forces [3–6] or a simplified energy density potential [7]. Note that different properties of nuclear matter, nuclear surface, and nuclei are well described in both the Hartree–Fock approximation and the energy density functional with effective Skyrme forces. The microscopic nuclear–nuclear double-folding potential is based on different parameterizations of nucleon–nucleon forces (M3Y, Reid, or Paris parameterizations) and nucleon densities of both nuclei [8–11].

Folding potentials and potentials of the Woods–Saxon type grow from large negative values at $R = 0$ with increasing distance R between the nuclei. The nuclear component of these potentials is therefore attractive at any distance between the nuclei. Unlike these potentials, the “proximity” potential [2], potentials based on Skyrme forces [3–6], and the simplified energy density functional in [7] are attractive at large and short distances between the interacting nuclei and repulsive at very short distances where the nuclei strongly overlap. The same behavior is typical for potentials calculated using modified M3Y [12] or nucleon–nucleon Reid soft core forces [13]. The repulsion of two colliding nuclei at short distances where the densities of these nuclei strongly overlap and are doubled in some volume is associated with the high incompressibility coefficient of nuclear matter, the contribution of kinetic energy into the potential, consideration of the Pauli principle, and antisymmetrization [3–6]. The contribution of antisymmetrization and the kinetic energy into the nucleus–nucleus potential is directly taken into account in the framework of semi-microscopic models using the energy density functional with Skyrme forces [4–6].

A large number of experimental data have been analyzed using the Woods–Saxon potential and the double-folding potential [1, 8–11]. However, very few reactions have been studied using the repulsive core potential at short distances [3–7, 12, 13]. In [15], elastic scattering reactions with the potential containing a parabolic repulsive core were studied. The contribution of the core into the potential was small, however; as a result, the potential at short distances remained attractive [15]. In other words, the analysis of characteristics of different reactions using the repulsive-core potential at short distances between nuclei is an interesting problem.

Repulsion takes place at short distances between interacting nuclei. The influence of the repulsive core can therefore be manifested in reactions sensitive to the potential value at short distances. It may be expected that the elastic scattering of "hard" nuclei $^{12}\text{C} + ^{12}\text{C}$ and $^{16}\text{O} + ^{12}\text{C}$ at energies above the barrier is sensitive to the potential value at these distances [8–11, 16, 17]. The data on elastic scattering for these systems at different energies above the barrier were obtained in [8, 9, 16] and analyzed in [8, 9, 11] using very deep double-folding and Woods–Saxon potentials. In [15], the reaction $^{16}\text{O} + ^{12}\text{C}$ was studied for the potential with a parabolic core; the depths of the attractive potential at short distances were considerably less than in [8, 9, 11]. The shallow potential determined using the folding method was used in [14] to describe the cross section of this reaction. The data on elastic scattering for $^{12}\text{C} + ^{12}\text{C}$ and $^{16}\text{O} + ^{12}\text{C}$ with the potential including a repulsive core were not analyzed.

POTENTIAL PARAMETERIZATION

The real component of the nucleus–nucleus potential $v(R)$ consists of the Coulomb $v_C(R)$, nuclear $v_N(R)$, and centrifugal $v_l(R)$ components:

$$v(R) = v_C(R) + v_N(R) + v_l(R). \quad (1)$$

For these components of the nucleus–nucleus potential, we propose the following expressions:

$$v_C(R) = \begin{cases} \frac{Z_1 Z_2 e^2}{R}, & R \geq R_C \\ \frac{Z_1 Z_2 e^2}{R} \left[\frac{3}{2} - \frac{R^2}{2R_C^2} \right], & R < R_C \end{cases} \quad (2)$$

$$v_N(R) = \begin{cases} \frac{-V_0}{1 + \exp[R - r_0(A_1^{1/3} + A_2^{1/3})/d_0]}, & R \geq R_m \\ b_0 + b_1 s + b_2 s^2 + b_3 s^3 + b_4 s^4, & R < R_m \end{cases} \quad (3)$$

$$v_l(R) = \frac{\hbar^2 l(l+1)}{2M[A_1 A_2 / (A_1 + A_2)] R^2}. \quad (4)$$

Here, $A_{1,2}$ and $Z_{1,2}$ are the numbers of nucleons and protons in the corresponding nuclei, e is the proton charge, M is the nucleon mass, $R_C = r_C(A_1^{1/3} + A_2^{1/3})$, $s = R - R_m$, and l is the orbital momentum. Taking into account that the value of the nuclear component of the potential and its derivative must be continuous at the matching point R_m , we find

$$\begin{aligned} b_0 &= \frac{-V_0}{1 + \exp[R_m - r_0(A_1^{1/3} + A_2^{1/3})/d_0]}, \\ b_1 &= \frac{V_0 \exp[R_m - r_0(A_1^{1/3} + A_2^{1/3})/d_0]}{d_0 \{1 + \exp[R_m - r_0(A_1^{1/3} + A_2^{1/3})/d_0]\}^2}. \end{aligned} \quad (5)$$

The imaginary component of the nuclear potential consists of the volume and surface components:

$$W(R) = -\frac{W_0}{1 + \exp[R - r_w(A_1^{1/3} + A_2^{1/3})/d_w]} - \frac{W_s \exp[R - r_s(A_1^{1/3} + A_2^{1/3})/d_s]}{d_s \{1 + \exp[R - r_s(A_1^{1/3} + A_2^{1/3})/d_s]\}^2}. \quad (6)$$

If the 14 following parameters are known— V_0 , r_0 , d_0 , b_2 , b_3 , b_4 , R_m , R_C , W_0 , r_w , d_w , W_s , r_s , and d_s —the angular distribution of the nuclear reaction can thus be described in the framework of the optical model. The first eight and the last six parameters are related, respectively, to the real and imaginary components of the potential.

ELASTIC SCATTERING

We find the 14 potential parameters by fitting the data for the elastic scattering reactions $^{12}\text{C} + ^{12}\text{C}$ and $^{16}\text{O} + ^{12}\text{C}$. For each collision energy, we find the set of parameters that results in the minimum value of

$$\chi^2 = \frac{1}{N} \sum_{i=1}^N \frac{(\sigma_{\text{calc}}(\theta_i) - \sigma_{\text{exp}}(\theta_i))^2}{\delta\sigma_{\text{exp}}(\theta_i)}, \quad \text{where } N \text{ is the number}$$

of experimental points, $\sigma_{\text{calc}}(\theta_i)$ and $\sigma_{\text{exp}}(\theta_i)$ are the theoretical and experimental values of the cross section for the angle θ_i , respectively, and $\delta\sigma_{\text{exp}}(\theta_i)$ is the corresponding error. In order to increase the weight of data at large angles, which are especially sensitive to the power and shape of the optical potential at short distances, we assume (as was done in [8, 9]) that for all data $\delta\sigma_{\text{exp}}(\theta_i) = 0.1\sigma_{\text{exp}}(\theta_i)$. The reactions $^{12}\text{C} + ^{12}\text{C}$ at beam energies of 139.5, 158.8 MeV [17] and $^{16}\text{O} + ^{12}\text{C}$ at ^{16}O beam energies of 132 MeV [8, 9] and 169 MeV [9] were considered, and the obtained values of the potential parameters are given in the table.

Figures 1 and 2 show the experimental data on elastic scattering for $^{16}\text{O} + ^{12}\text{C}$ and $^{12}\text{C} + ^{12}\text{C}$ systems and the fitting results using the optical model for the repulsive-core potential for different energies. The real components of repulsive-core nucleus–nucleus potentials (1)–(6) for $l = 0$ (parameters for different collision energies are taken from the table) are shown in Fig. 3. The potential has a repulsive core at short distances; the well, at intermediate distances between the nuclei (see Fig. 3). The depth of the well V_{well} at the distance R_{well} is the minimum value of the potential.

Figures 1 and 2 show the results from calculations using the optical model for the repulsive-core potential (solid line) and for the potential without a repulsive core (dashed line) in order to demonstrate the influence of the repulsive core. The potential without a core for these calculations coincides with the corresponding repulsive-core potential at distances $R \geq R_{\text{well}}$ and is equal to V_{well} for $R < R_{\text{well}}$. The influ-

Parameters of optical potential for systems $^{12}\text{C} + ^{12}\text{C}$ и $^{16}\text{O} + ^{12}\text{C}$

| | $^{12}\text{C} + ^{12}\text{C}$ | $^{16}\text{O} + ^{12}\text{C}$ | | |
|------------------------|---------------------------------|---------------------------------|--------|--------|
| E_{lab} , MeV | 139.5 | 158.8 | 132 | 169 |
| V_0 , MeV | 35.692 | 35.921 | 37.258 | 39.092 |
| r_0 , fm | 1.104 | 1.096 | 0.967 | 1.048 |
| d_0 , fm | 0.719 | 0.767 | 0.851 | 0.761 |
| b_2 , MeVfm $^{-2}$ | -3.239 | -3.742 | -3.721 | -3.132 |
| b_3 , MeVfm $^{-3}$ | 7.453 | 4.794 | 6.391 | 5.854 |
| b_4 , MeVfm $^{-4}$ | 2.615 | 2.166 | 1.850 | 2.232 |
| R_m , fm | 4.441 | 4.568 | 6.341 | 5.717 |
| R_C , fm | 5.467 | 5.848 | 4.946 | 6.123 |
| W , MeV | 20.371 | 16.915 | 15.009 | 18.302 |
| r_w , fm | 0.808 | 0.934 | 1.104 | 1.102 |
| d_w , fm | 1.030 | 1.057 | 0.337 | 0.366 |
| W_s , MeV | 8.861 | 5.796 | 7.634 | 10.109 |
| r_s , fm | 1.192 | 1.280 | 1.313 | 1.278 |
| d_s , fm | 0.492 | 0.475 | 0.388 | 0.436 |
| σ^a , mb | 1414 | 1519 | 1364 | 1399 |
| χ^2 | 8.9 | 7.72 | 16.2 | 16.3 |

Note: ^a Total reaction cross section.

ence of the repulsive core can be seen from a comparison of the results in Figs. 1 and 2. Due to internal repulsion, the cross section increases considerably at backward angles, while at forward angles it is virtually identical for both types of potentials. The values of the total cross section of the reaction $^{16}\text{O} + ^{12}\text{C}$ given in the table are close to the corresponding values in [9]. Note that the internal core of the potential does not influence the values of the total reaction cross sections.

The values of χ^2 obtained for the repulsive-core potential (see table) are close to the corresponding values in [9, 11]. The quality of the descriptions obtained in [9, 11] is thus comparable. The value of χ^2 presented in [14] for the reaction $^{16}\text{O} + ^{12}\text{C}$ is, in contrast, much larger than the one we obtained, as can be seen from the table and [9].

POTENTIAL

Figure 3 compares repulsive-core nucleus–nucleus potentials (1)–(6) for $l = 0$ (with the parameters for different collision energies taken from the table) and the “proximity” [2] and semi-microscopic [4] potentials. The depth of the well for the repulsive-core potential depends on the collision energy. The depth of the well for the semi-microscopic potential is less than for the phenomenological repulsive-core potential. The potentials in [2, 4] and the repulsive-core potential are close at short distances; at great distances

between nuclei, however, the “proximity” potential is more attractive.

The semi-microscopic potential and the repulsive-core potentials obtained for different collision energies leads to close values of the barrier energy. The position of the well minimum obtained for different collision energies is $R \approx 3.5$ fm for the reaction $^{16}\text{O} + ^{12}\text{C}$ and $R \approx 2$ fm for the reaction $^{12}\text{C} + ^{12}\text{C}$. The repulsive core is present at distances $R \leq 2$ fm for any potential (Fig. 3). The distance at which the densities of the colliding nuclei noticeably overlap and as a result, the incompressibility of the nuclear matter and the Pauli principle result in strong repulsion, are therefore similar for all potentials. The values of the potential depth obtained in [9, 11] for different energies were in the interval from 170 to 362 MeV. Compared to these values, the depth of the phenomenological repulsive-core potentials proposed for describing elastic scattering $^{12}\text{C} + ^{12}\text{C}$ and $^{16}\text{O} + ^{12}\text{C}$ (see Fig. 3), is not large; i.e., the corresponding potentials are shallow.

NEARSIDE AND FAR SIDE CROSS SECTION COMPONENTS

Fuller's method [18] allows us to decompose the scattering trajectory into nearside and farside components. In this case, the scattering for which the nuclei touch one another on the same side onto which the scattering beam is deflected corresponds to the nearside component. The scattering for which the nuclei touch one another on one side and the scattering beam is deflected to the opposite side corresponds to the farside component.

Fuller's method [18] was used in [8, 9, 11] to demonstrate that the cross section of elastic scattering $^{12}\text{C} + ^{12}\text{C}$ and $^{16}\text{O} + ^{12}\text{C}$ at forward angles is determined by the nearside component, while the cross section for large and backward angles is determined by the farside component. The farside component is associated with the rainbow phenomenon [11] as a result of the refraction of the incident wave due to the strong attractive (very deep) nucleus–nucleus potential.

Figures 1 and 2 show the nearside and farside components of the elastic scattering amplitude for $^{12}\text{C} + ^{12}\text{C}$ and $^{16}\text{O} + ^{12}\text{C}$ obtained using repulsive-core potentials and potentials without a repulsive core. It can be seen from Fig. 1 that for reaction $^{16}\text{O} + ^{12}\text{C}$, the nearside component basically describes the cross section over the angular range, while the farside component is responsible for the structure of oscillations due to the interference of the nearside and farside components only. For reaction $^{12}\text{C} + ^{12}\text{C}$ (see Fig. 2), the nearside component is important at forward and backward angles; the farside component, at intermediate and backward angles. Due to the presence of a repulsive core, the values of the nearside and farside components of the scattering amplitude increase at backward angles.

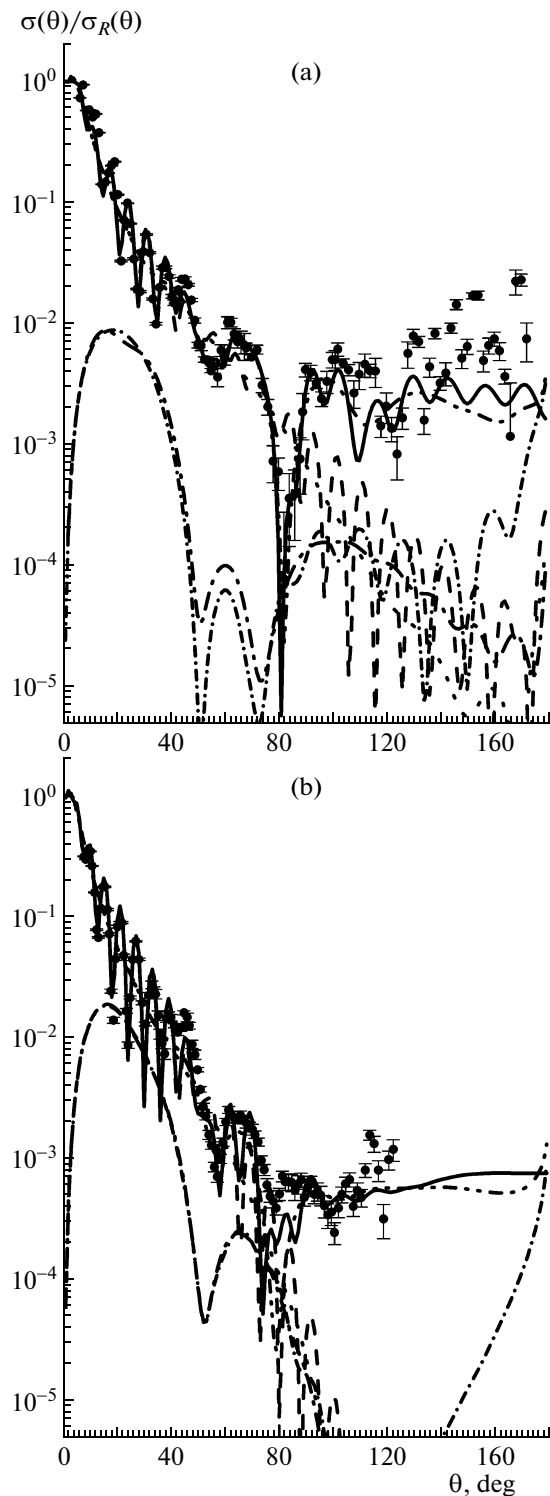


Fig. 1. Data on elastic scattering $^{16}\text{O} + ^{12}\text{C}$ for ^{16}O beam energies of (a) 132 MeV and (b) 169 MeV and calculations using the optical model. Circles show the experimental data. Solid, dashed/double-dotted, and dashed/dotted lines show the cross sections for the total, nearside, and farside components of elastic scattering amplitude, respectively, calculated for repulsive-core potential. Dashed, dotted, and dashed/dotted lines show the analogous cross sections calculated for the potentials without a repulsive core.

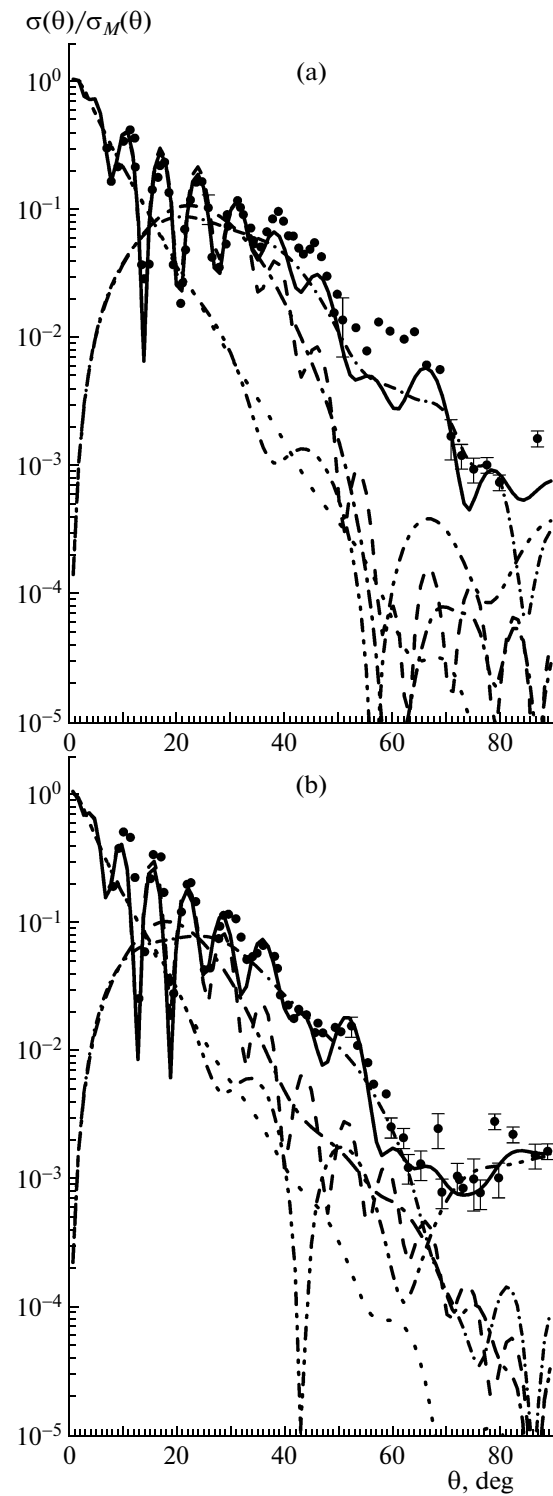


Fig. 2. Data on elastic scattering $^{12}\text{C} + ^{12}\text{C}$ for energies of (a) 139.5 MeV and (b) 158.8 MeV, and for calculations using the optical model. Notation for the curves is the same as in Fig. 1.

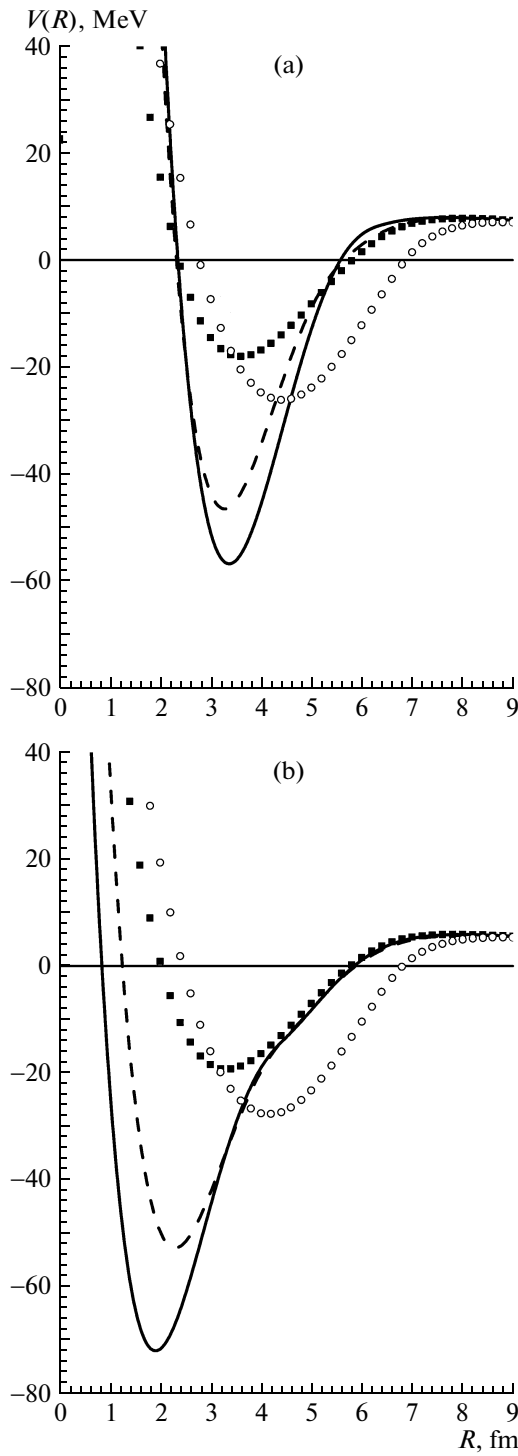


Fig. 3. Repulsive-core potential determined for elastic scattering: (a) $^{16}\text{O} + ^{12}\text{C}$ for ^{16}O beam energy of (solid curve) 132 MeV and (dashed curve) 169 MeV; (b) $^{12}\text{C} + ^{12}\text{C}$ for (solid curve) 139.5 MeV and (dashed curve) 158.8 MeV. The following potentials are also shown for comparison: (circles) “proximity” [2] and (squares) semi-microscopic [4] potentials.

CONCLUSIONS

It was shown that the data on elastic scattering for $^{12}\text{C} + ^{12}\text{C}$ and $^{16}\text{O} + ^{12}\text{C}$ can be described using a shallow phenomenological repulsive-core potential. Due to the presence of a repulsive core at distances $R \leq 2$ fm, the values of the nearside and farside components of the scattering amplitude grow strongly for backward angles, leading to enhancement of elastic scattering cross sections in this angular region.

REFERENCES

1. Frobrich, P. and Lipperheide, R., *Theory of Nuclear Reactions*, Oxford: Clarendon Press, 1996.
2. Blocki, J., Randrup, J., Swiatecki, W.J., and Tang, C.F., *Ann. Phys.*, New York, 1977, vol. 105, p. 427.
3. Brink, D.M. and Stancu, F., *Nucl. Phys. A*, 1976, vol. 270, p. 236.
4. Denisov, Yu.V., *Phys. Lett. B*, 2002, vol. 526, p. 315.
5. Denisov, Yu.V. and Norenberg, W., *Eur. Phys. J. A*, 2002, vol. 15, p. 375.
6. Denisov, V.Yu. and Nesterov, V.A., *Phys. At. Nucl.*, 2006, vol. 69, p. 1472.
7. Brueckner, K.A., Buchler, J.R., and Kelly, M.M., *Phys. Rev. C*, 1969, vol. 173, p. 994.
8. Ogloblin, A.A., Khoa Dao, T., Kondo, Y., et al., *Phys. Rev. C*, 1998, vol. 57, p. 1797.
9. Ogloblin, A.A., Glukhov, Yu.A., Trzaska, W.H., et al., *Phys. Rev. C*, 2000, vol. 62, p. 044601.
10. Soubbotin, V.B., et al., *Phys. Rev. C*, 2001, vol. 64, p. 014601.
11. Brandan, M.E. and Satchler, G.R., *Phys. Rep.*, 1997, vol. 285, p. 1797; Khoa Dao, T., von Oertzen, W., Bohlen, H.G., and Ohkubo, S., *J. Phys. G*, 2007, vol. 34, p. R111; Brandan, M.E., *Phys. Rev. Lett.*, 1988, vol. 60, p. 784.
12. Misicu, S. and Esbensen, H., *Phys. Rev. C*, 2007, vol. 75, p. 034606.
13. Izumoto, T., Krewald, S., and Faessler, A., *Nucl. Phys. A*, 1980, vol. 341, p. 319.
14. Hossain, S., Abdullah, M.N.A., Hasan, K.M., et al., *Phys. Lett. B*, 2006, vol. 636, p. 248.
15. Gridnev, K.Ya., Rodionova, E.E., and Fadeev, S.N., *Yadern. Fiz.*, 2008, vol. 71, p. 1262 [*Phys. Atomic Nuclei* (Engl. Transl.), 2008, vol. 71, no. 7, p. 1262].
16. Dem'yanova, A.S., private communication.
17. Kubono, S., et al., *Phys. Lett. B*, 1985, vol. 163, p. 75.
18. Fuller, R.C., *Phys. Rev. C*, 1975, vol. 12, p. 1561.